

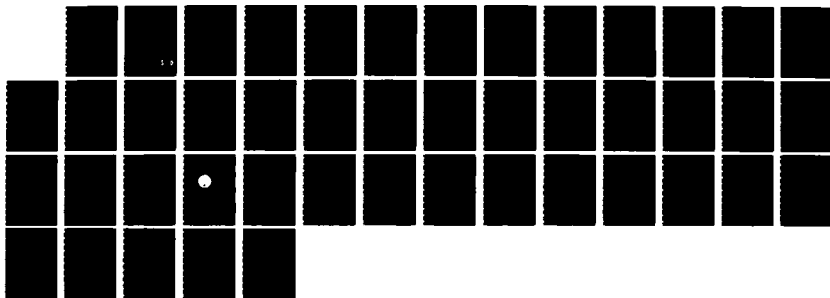
AD-A172 739

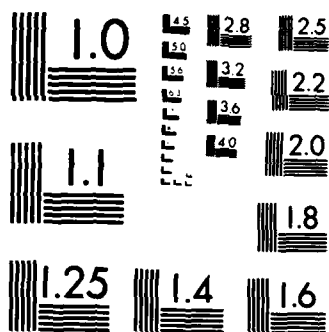
THE INFLUENCE OF ELECTRIC CURRENT ON CRACK PROPAGATION  
IN THERMAL FATIGUE (U) CARNEGIE-MELLON UNIV PITTSBURGH  
PA DEPT OF MECHANICAL ENGINEE J H GRIFFIN 17 FEB 86  
1-52113 AFOSR-TR-86-0886 AFOSR-84-0203 F/G 11/6

1/1

UNCLASSIFIED

NL






MICROCOPY RESOLUTION TEST CHART  
NATIONAL BUREAU OF STANDARDS-1963-A

UNCLASSIFIED

SECURITY CLASSIFICATION OF THIS PAGE

(2)

## REPORT DOCUMENTATION PAGE

1a. REPORT SECURITY CLASSIFICATION <b>UNCLASSIFIED</b>			1b. RESTRICTIVE MARKINGS													
2a. SECURITY CLASSIFICATION AUTHORITY			3. DISTRIBUTION/AVAILABILITY OF REPORT  Approved for public release, distribution unlimited													
2b. DECLASSIFICATION/DOWNGRADING SCHEDULE																
4. PERFORMING ORGANIZATION REPORT NUMBER(S)  1-52113			5. MONITORING ORGANIZATION REPORT NUMBER(S)  <del>F02671-8401</del> <b>AFOSR-TR. 86-0886</b>													
6a. NAME OF PERFORMING ORGANIZATION Carnegie-Mellon University Mechanical Engineering Dept.		6b. OFFICE SYMBOL (If applicable)	7a. NAME OF MONITORING ORGANIZATION Air Force Office of Scientific Research													
6c. ADDRESS (City, State and ZIP Code) Schenley Park Pittsburgh, PA 15213			7b. ADDRESS (City, State and ZIP Code) Building 410 Bolling AFB, D.C. 20332-6448													
8a. NAME OF FUNDING/SPONSORING ORGANIZATION <b>AFOSR</b>		8b. OFFICE SYMBOL (If applicable) <b>AFOSR/PMB</b>	9. PROCUREMENT INSTRUMENT IDENTIFICATION NUMBER AFOSR-84-0203													
8c. ADDRESS (City, State and ZIP Code) <del>AFOSR/PMB</del> Building 410 Bolling AFB, D.C. 20332-6448			10. SOURCE OF FUNDING NOS. <table border="1"> <tr> <th>PROGRAM ELEMENT NO.</th> <th>PROJECT NO.</th> <th>TASK NO.</th> <th>WORK UNIT NO.</th> </tr> <tr> <td>61102F</td> <td>2307</td> <td>B2</td> <td></td> </tr> <tr> <td></td> <td>2302</td> <td></td> <td></td> </tr> </table>		PROGRAM ELEMENT NO.	PROJECT NO.	TASK NO.	WORK UNIT NO.	61102F	2307	B2			2302		
PROGRAM ELEMENT NO.	PROJECT NO.	TASK NO.	WORK UNIT NO.													
61102F	2307	B2														
	2302															
11. TITLE (Include Security Classification) The Influence of Electric Current on Crack Propagation in Thermal Fatigue Tests																
12. PERSONAL AUTHOR(S) Professor Jerry H. Griffin																
13a. TYPE OF REPORT Final		13b. TIME COVERED FROM 8/1/84 TO 7/31/85	14. DATE OF REPORT (Yr., Mo., Day) 86/2/17	15. PAGE COUNT 43												
16. SUPPLEMENTARY NOTATION																
17. COSATI CODES <table border="1"> <tr> <th>FIELD</th> <th>GROUP</th> <th>SUB. GR.</th> </tr> <tr> <td></td> <td></td> <td></td> </tr> </table>			FIELD	GROUP	SUB. GR.				18. SUBJECT TERMS (Continue on reverse if necessary and identify by block number) Elastic fracture mechanics, electric heating, thermal stresses							
FIELD	GROUP	SUB. GR.														
19. ABSTRACT (Continue on reverse if necessary and identify by block number) This report discusses the work accomplished during the AFOSR Grant AFOSR-84-0203, entitled "The Influence of Electric Current on Crack Propagation in Thermal Fatigue Tests." The goal of this work was to develop a method for estimating the crack tip stresses that result from a non-uniform temperature distribution near the crack tip that occurs when resistance heating is used to thermally cycle fatigue specimens.																
<div style="display: flex; justify-content: space-between; align-items: center;"> <div>DTIC FILE COPY</div> <div style="text-align: right;">  </div> </div>																
20. DISTRIBUTION/AVAILABILITY OF ABSTRACT UNCLASSIFIED/UNLIMITED <input checked="" type="checkbox"/> SAME AS RPT. <input type="checkbox"/> DTIC USERS <input type="checkbox"/>			21. ABSTRACT SECURITY CLASSIFICATION <b>D</b> UNCLASSIFIED													
22a. NAME OF RESPONSIBLE INDIVIDUAL Professor Jerry H. Griffin <b>GEORGE K. HABITCO, MAJUR</b>			22b. TELEPHONE NUMBER (Include Area Code) <b>767-4121268-3860 4935</b>	22c. OFFICE SYMBOL <b>NA</b>												

405494 rtm

**AFOSR-TR- 86 - 0886**

# **THE INFLUENCE OF ELECTRIC CURRENT ON CRACK PROPAGATION IN THERMAL FATIGUE TESTS**

**AIR FORCE OFFICE OF SCIENTIFIC RESEARCH (AFSC)  
NOTICE OF TRANSMITTAL TO DTIC**  
This technical report has been reviewed and is  
approved for public release IAW AFR 190-12.  
Distribution is unlimited.  
**MATTHEW J. KENNEY**  
Chief, Technical Information Division

## **FINAL REPORT**

Approved for public release;  
distribution unlimited.

### **Submitted to**

**Air Force Office of Scientific Research  
Bolling Air Force Base  
Washington, D.C. 20332**

### **Submitted by**

**J. H. Griffin and S. Cunningham  
Department of Mechanical Engineering  
Carnegie-Mellon University  
Pittsburgh, Pennsylvania 15213**

**February 1986**

## Table of Contents

1 INTRODUCTION	1
2 ELECTRIC POTENTIAL PROBLEM	7
2.1 Formulation	7
2.2 Determining the Boundary Condition, $f(O)$	8
2.3 Solution	8
3 THERMOELASTICITY PROBLEM	9
3.1 Formulation	9
3.2 Solution	12
4 RESULTS	14
5 DISCUSSION	16



A-1



## 1 INTRODUCTION

This report discusses the work accomplished during the AFOSR Grant AFOSR-84-0203, entitled "The Influence of Electric Current on Crack Propagation in Thermal Fatigue Tests." The goal of this work was to develop a method for estimating the crack tip stresses that result from a non-uniform temperature distribution near the crack tip that occurs when resistance heating is used to thermally cycle fatigue specimens.

A problem associated with thermal fatigue tests is obtaining sufficiently rapid thermal cycles in the test specimens. In order to overcome this problem, large electric currents are often used to cyclically heat the samples since this mode of heating can be easily controlled and rapidly cycled. However, in the presence of an open crack an otherwise uniform electric field is disturbed, causing a  $1/\sqrt{r}$  singularity in the current which results in localized heating at the crack tip. Thus, cracked thermal fatigue specimens which are electrically heated have a distinctly non-uniform temperature field with the crack tip acting as a heat source in the material.

Recently, experiments were conducted through a program sponsored jointly by the Air Force Wright Aeronautical Research Laboratories and the Defense Advanced Research Projects Agency. The aim of the experiments was to address the impact of simultaneous variations in temperature and stress on crack growth predictions [1]. Temperature variations were achieved by application of a 60 Hz a.c. current. Comparison of results obtained on samples which were thermomechanically fatigued out-of-phase (temperature and load cycles were  $180^\circ$  out of phase) to those fatigued in-phase showed a significantly greater crack growth associated with the in-phase testing, while no discernible difference between the crack growth rates of out-of-phase and isothermally tested samples was observed. An additional outcome of the testing is a distinct difference in crack growth behavior between specimens tested out-of-phase and those tested either isothermally or in-phase. The out-of-phase samples exhibited significant shear lips while those tested isothermally and in-phase exhibited flat crack faces.

A possible explanation for the anomalous crack growth behavior is that thermal stresses caused by the resistance heating were not taken into account in calculations of stress intensities. It is the goal of this work to estimate the contribution of the electric field to the stress intensity as induced by the associated quasi-static temperature field to estimate the magnitude of its contribution under test conditions.

The problem of analytically determining the mechanical state of the crack tip in an electrically heated specimen requires the solution of two interrelated problems: determining the disturbed electric field in the crack region from which heat generation can be calculated and secondly, using the heat generation as a heat source in the thermoelasticity problem to calculate the stress field.

The electric field problem has been of interest in fracture mechanics because of its role in the widely used electric potential technique for monitoring fatigue crack growth. Analytical, experimental and numerical procedures have been developed to determine suitable calibration curves which relate the potential drop across the crack to the crack length, see, for example, references [2-6]. The analytical expressions generally use the analogy of fluid flow around a flat plate and a mapping technique such as the Schwarz-Christoffel technique used in the present analysis [7].

The thermoelastic problem is more complex. The estimation of thermoelastic stresses induced by a heat source at the tip of a crack requires determining the solution to Poisson's equation to obtain the stationary temperature field and the solution to the nonhomogeneous biharmonic equation to obtain the stresses due to the temperature field. The latter part uses the Duhamel-Neumann analogy and associated modified Airy stress function to separate the nonuniform temperature distribution from the elasticity problem [8-10].

The first work dealing with the two-dimensional thermal stress fields associated with cracks was published by Florence and Goodier [11] and Sih [12]. The method of complex representation of the elastic state was used to derive the theoretical stress intensity factors in infinite two-dimensional cracked regions for both the symmetric and antisymmetric problem classes. Sih gives the thermal stress components near the crack tip (for the geometry in Figure 1, neglecting higher order terms) as

$$\sigma_x = \frac{K_1}{\sqrt{2r}} \cos \frac{\theta}{2} \left( 1 - \sin \frac{\theta}{2} \sin \frac{3\theta}{2} \right) - \frac{K_2}{\sqrt{2r}} \sin \frac{\theta}{2} \left( 2 + \cos \frac{\theta}{2} \cos \frac{3\theta}{2} \right) \quad (1)$$

$$\sigma_y = \frac{K_1}{\sqrt{2r}} \cos \frac{\theta}{2} \left( 1 + \sin \frac{\theta}{2} \sin \frac{3\theta}{2} \right) + \frac{K_2}{\sqrt{2r}} \sin \frac{\theta}{2} \cos \frac{\theta}{2} \cos \frac{3\theta}{2} \quad (2)$$

$$\tau_{xy} = \frac{K_1}{\sqrt{2r}} \sin \frac{\theta}{2} \cos \frac{\theta}{2} \cos \frac{3\theta}{2} + \frac{K_2}{\sqrt{2r}} \cos \frac{\theta}{2} (1 - \sin \frac{\theta}{2} \sin \frac{3\theta}{2}) \quad (3)$$

where

$$K_1 = \frac{2}{\sqrt{a}} \operatorname{Re}[A] \quad (4)$$

is the symmetric stress intensity factor,

$$K_2 = \frac{-2}{\sqrt{a}} \operatorname{Im}[A] \quad (5)$$

is the antisymmetric stress intensity factor and  $A$  is a complex constant which depends on crack configuration and the form of the prescribed temperature constraints.

These expressions are identical to the general elastic crack-tip stress field given by Irwin [13] for traction boundary condition problems. With some manipulation, the corresponding stress distribution in terms of polar coordinates can be written using identities given by [14] as:

$$\sigma_r = \frac{K_1}{4\sqrt{2r}} (5 \cos \frac{\theta}{2} - \cos \frac{3\theta}{2}) - \frac{K_2}{4\sqrt{2r}} (5 \sin \frac{\theta}{2} - 3 \sin \frac{3\theta}{2}) \quad (6)$$

$$\sigma_\theta = \frac{K_1}{4\sqrt{2r}} (3 \cos \frac{\theta}{2} + \cos \frac{3\theta}{2}) - \frac{K_2}{4\sqrt{2r}} (3 \sin \frac{\theta}{2} + \sin \frac{3\theta}{2}) \quad (7)$$

$$\tau_{r\theta} = \frac{K_1}{4\sqrt{2r}} (\sin \frac{\theta}{2} + \sin \frac{3\theta}{2}) + \frac{K_2}{4\sqrt{2r}} (\cos \frac{\theta}{2} + 3 \cos \frac{3\theta}{2}) \quad (8)$$

where  $K_1$  and  $K_2$  are as defined above.

An alternative formulation for this class of problems was presented by Bapu Rao [15] for determining the state of thermal stresses in an insulated crack in an infinite thin plate subjected to uniform heat flow. In this case, both the stationary temperature and stress problems were formulated in the elliptic coordinate system and the solution developed completely in elliptic coordinates using biharmonic



functions and then the results were transformed through a series expansion to polar coordinates with the crack tip as the origin. The final results obtained for the local stresses at the crack tip in polar coordinates agree completely with those obtained by Sih. It is noted that the real parts of the stress field are identical to the singular terms of the Williams' eigenfunction relations expressed by Torvik [16,17].

Experiments performed by Svoboda [18] showed good agreement between the stress field corresponding to uniform heat flow presented in [12] and experimental data. The test specimens used were made of plexiglas since this material is essentially brittle, can be prepared easily and is relatively isotropic. In this case, the complex constant,  $A$ , corresponded closely to that obtained by Sih for the antisymmetric, uniform temperature field case:

$$A = \frac{iG\alpha a^2 \sin \gamma}{(1 + \nu_0)} \bullet \nabla T \quad (9)$$

where  $\alpha$  is the thermal expansion coefficient,  $\nu_0$  is an elastic constant ( $\nu_0 = 3 - 4\nu$ , plane strain,  $\nu_0 = (3 - \nu)/(1 + \nu)$ , plane stress),  $a$  is half the crack length, and  $\nabla T$  is the undisturbed temperature gradient directed at an arbitrary angle  $\gamma$  with respect to the crack axis.

Thus, estimating the stress field induced by electric current flow around a crack reduces to determining the coefficient of the singular term in Williams' eigenfunction series caused by the symmetric temperature field induced by the electric current. In addition, the solution to the elasticity problem must satisfy appropriate boundary conditions. In the problem considered herein the boundaries will be considered traction free, consequently, any stresses that are calculated exist in addition to those induced by mechanical loading.

Because of the complicated form of the boundary conditions in elasticity problems, closed-form solutions to problems of cracks in finite regions are rarely obtained. Several investigators have studied the problem of thermoelastic stresses due to various temperature fields in cracked regions. Konishi and Atsumi [19] used the method of integral equations to numerically solve the antisymmetric uniform heat flow/insulated line crack problem for a semi-infinite strip with the crack parallel to the surface. Their results revealed a stress intensity factor proportional to the temperature gradient times the crack length to the 3/2 power, consistent with Sih's result.

Sekine [20,21] also studied the two-dimensional insulated line crack/uniform heat flow problem in a semi-infinite strip with the crack arbitrarily oriented. In [20], the temperature was prescribed on the surface of the crack and the crack was modelled as continuous distributions of heat sources and edge dislocations. Singular integral equations were derived and the solution obtained is in the form of the product of the series of Tchebycheff polynomials and their weight functions. In [21], the corresponding problem for a thermally insulated line crack was solved by introducing a continuous distribution of sources of temperature discontinuity rather than that of heat sources. Similarly, Tchebycheff polynomial series were obtained. The coefficients of the polynomials were determined by solving the set of linear algebraic equations. The stress intensity factors for the symmetric and antisymmetric types were numerically evaluated and compared graphically. The results for the limiting case when the crack is situated extremely far from the surface are, again, in complete agreement with Sih. The results for the case when the uniform heat flow is perpendicular to the plane of the crack are in agreement with Konishi and Atsumi.

Other geometry and temperature field two-dimensional crack problems have been studied. Sekine [22] also studied the problem of a heated bounding surface and solved it numerically again using singular integral equations and Tchebycheff polynomials. Tweed and Lowe [23] used transform techniques to reduce the general problem of a crack in a half-plane to that of solving integral equations. The point source problem, was solved numerically for a hollow cylinder of infinite length by Herrmann and Kuemmerling [24] by using singular integral equations. They emphasized that for cracks of large length where the surfaces strongly influence the stress intensity, this numerical method is inappropriate and suggested using finite-element or the well known J-integral (a note on the use of the J-integral for thermal stress problems is in [25]).

Finally, Sumi and Katayama [26] studied thermal stresses at crack tips in finite plates. Their results, for both symmetric and antisymmetric cases were obtained by evaluating the unknown coefficients in the eigenfunction series using a modified mapping collocation method.

The role of electric current in thermo-mechanical fatigue tests has previously not been established. The presence of the crack causes a singularity in the electric current which, because of resistance heating, induces an even more severe singularity in the heat flux at the crack tip. This singular heat source can lead to significant

temperature gradients which are not being taken into consideration by temperature measurements made at some finite distance from the crack tip. Thus, one goal of the current work is to establish the magnitude of the temperature gradient near the crack tip in order to estimate errors that can occur in measuring crack tip temperatures. The temperature field that results from the singular heat flux also gives rise to thermal stresses which load the crack tip. These stresses will affect how the crack propagates. Thus, a second goal of this work is to establish a method for estimating the crack tip stresses that are induced by the current/crack interaction.

In order to establish these estimates of crack tip temperature and stresses in a form which is easily applicable to a variety of materials, the problem is simplified in the following manner, enabling relatively simple closed form solutions. The specimen which is heated electrically may have the edge crack geometry of Figure 2. The problems that will be analyzed will be concerned with the circular subregion ( $R_a$  of Fig. 2) of radius 'a' which surrounds the crack tip. The electric potential in this region is assumed to be the same as that which occurs for a crack in an infinitely wide plate. The current terms that are singular are extracted from the infinite plate solution by representing the solution in terms of the eigenfunctions associated with the cracked circular plate. The temperatures in the cracked circular plate are calculated based on three assumptions: the temperature is a constant reference value on the outer boundary, the crack acts as a perfect insulator, and the region is heated only by the singular heat flux term. Once the temperature field is determined, the thermal stress fields in the cracked circular plate are calculated under the assumption that its boundaries are traction free. The thermal stress problem is solved using Williams' stress functions which satisfy the boundary conditions on the crack face and which are numerically made to satisfy the boundary conditions on the outer boundary in a least squares sense. Only the lowest order stress function gives rise to singular crack tip stresses and its coefficient is proportional to K, the 'stress intensity' parameter commonly used in fracture mechanics to assess damage. Thus, the solution results in a relatively simple expression for estimating the stress intensity induced by local heating of the crack tip that can occur while using electric currents to heat thermal fatigue specimens.

Stress intensity factors for some nickel alloys are calculated using the data presented in [1], and are compared with the stress intensity factors induced by an isothermal mechanical fatigue specimen of the same type. The results show the

thermal stress intensity induced by the electric current is significant and is additive and therefore can contribute to an increased crack growth rate in electrically heated thermal-mechanical fatigue tests.

## 2 ELECTRIC POTENTIAL PROBLEM

The electric potential problem is solved for the model problem. First the electrical potential over the circular region is established through a mapping technique. From this, the boundary condition,  $E(a, \theta) = f(\theta)$  is determined for the circular region containing the crack. The boundary condition is then used to numerically evaluate the Fourier coefficients in an eigenfunction representation of the electric potential. This approach isolates the term that causes a singular heat flux at the crack tip. It is the contribution of this singular heat source to the thermoelastic stress field which will be evaluated in this report.

### 2.1 Formulation

Two regions are first defined (see Figure 2).  $R_s$  corresponds to the circular region surrounding the semi-crack in which the thermoelastic problem will be solved, while  $R_o$  is the complementary region of the plate, not including  $R_s$ .

$$R_s = \{(r, \theta) \mid 0 < r < a, -\pi < \theta < \pi\}$$

$$R_o = \{(x, y) \mid 0 < x < \frac{W}{2}, -\frac{L}{2} < y < \frac{L}{2}, x, y \notin R_s\}$$

The electric potential problem is then stated: determine  $E(r, \theta)$  such that

$$\nabla^2 E(r, \theta) = 0 \text{ on } R_s \quad (10)$$

and satisfying the boundary conditions

$$E(a, \theta) = f(\theta),$$

where  $f(\theta)$  is determined below. The condition of perfect insulation (no current flow) across the crack requires

$$\frac{\partial E}{\partial \theta}(r, \pi) = \frac{\partial E}{\partial \theta}(r, -\pi) = 0 \quad (11)$$

Finally, the potential must also be bounded at the crack tip,

$$|E(r, \theta)| < M \text{ as } r \rightarrow 0 \quad (12)$$

## 2.2 Determining the Boundary Condition, $f(\theta)$

In order to establish the appropriate boundary condition, a Schwarz-Christoffel conformal mapping is used. From [7], the solution to the problem of uniform flow about a flat plate is given by the complex potential

$$\Psi(z) = V_0 (z^2 + a^2)^{1/2} = \phi(x, y) + i\psi(x, y) \quad (13)$$

here  $\phi(x, y)$  is the velocity potential,  $\psi(x, y)$  is the stream function,  $V_0$  is the far field velocity and  $z = x + iy$ . The fluid problem is analogous to the electric potential problem where  $V_0$  is equivalent to  $E_0/L$  ( $E_0$  is the applied voltage and  $L$  the specimen length). The electric potential is analogous to the velocity potential which is the real part of  $\Psi(z)$ . Thus, to find the potential on the boundary  $r = a$ , the complex geometry in Figure 3 is used:

$$\phi(x, y) = \text{Re}[\Psi] = \frac{E_0}{L} \sqrt{\rho_1 \rho_2} \cos \left( \frac{\theta_1 + \theta_2}{2} \right) \quad (14)$$

where  $\rho_1, \rho_2, \theta_1, \theta_2$  are defined by Figure 3. On the boundary  $r = a$ ,

$$\begin{aligned} \phi|_a &= \frac{E_0}{L} \sqrt{5 + 4 \cos \theta} \cos \left\{ \frac{1}{2} \left[ \theta + \frac{\pi}{2} + \arccos \left( \frac{-\sin \theta}{\sqrt{5 + 4 \cos \theta}} \right) \right] \right\} \cdot a \\ &= f(\theta) \end{aligned} \quad (15)$$

## 2.3 Solution

The solution to the electric potential problem is expressed in terms of the eigenfunctions of the problem by using the separation of variables technique:

$$E(r, \theta) = R(r)\Theta(\theta) \quad (16)$$

Problem symmetry leads to

$$E(r, \theta) = C_n + \sum_{n=1}^{\infty} C_n r^{n/2} \cos n(\theta - \pi)/2 \quad (17)$$

The electric potential within the circular region is obtained by determining the

coefficients in the Fourier cosine series. Since the functions are orthogonal, the coefficients can be evaluated directly,

$$C_n = \frac{a^{(2-n)/2}}{\pi} \int_{-\pi}^{\pi} \cos \frac{n(\theta - \pi)}{2} f(\theta) d\theta \quad (18)$$

by performing the integration numerically. Results of this numerical integration are tabulated in Table 1 for values of  $n$  up to 32. Neglecting higher order terms, the first coefficient (singular current coefficient) gives an expression for potential as a function of  $r$  and  $\theta$ :

$$E(r, \theta) = \sqrt{\frac{E_0}{2ar}} \cos(\theta - \pi/2) \quad (19)$$

It is this component of the electric potential which gives rise to the dominant (singular) heat source at the crack tip and, consequently, it is the contribution of this term which is evaluated in this report.

### 3 THERMOELASTICITY PROBLEM

Once the potential over the plate is obtained, the heat flux in the circular region can be determined. From this, the thermoelasticity problem, which includes finding the temperature field, is formulated using the Duhamel-Neumann analogy to model the problem as one with a constant temperature field. Using this approach, an Airy stress function formulation may be used in which the temperature field produces surface tractions and body forces. The solution to the resulting non-homogeneous biharmonic equation is determined using standard techniques. The solution to the homogeneous part is represented in terms of Williams' eigenfunctions, the coefficients of which are evaluated numerically. The coefficient of the lowest Williams' eigenfunction establishes the magnitude of the singular stress field at the crack tip, and it is this quantity which we seek to evaluate.

#### 3.1 Formulation

##### A. The Temperature Field

The heat flux,  $h(r, \theta)$ , induced by the current is

$$h(r, \theta) = \sigma(\nabla E \cdot \nabla E) \quad (20)$$

where  $\sigma$  is the electrical conductivity. For steady-state temperature fields, the local temperature variation,  $T(r, \theta)$ , is related to the heat flux by

$$\nabla^2 T(r, \theta) = - \frac{h(r, \theta)}{k} \quad (21)$$

where  $k$  is the thermal conductivity.

The temperature field must satisfy the condition of a constant reference temperature at the edge

$$T = T_0 \text{ on } r = a, \quad -\pi < \theta < \pi \quad (22)$$

perfect insulation across the crack requires

$$\frac{\partial T}{\partial \theta}(r, -\pi) = \frac{\partial T}{\partial \theta}(r, \pi) = 0, \quad 0 < r < a, \quad (23)$$

finally, the temperature must remain bounded in the limit as  $r$  approaches zero,

$$|T(r, \theta)| < M \text{ as } r \rightarrow 0. \quad (24)$$

## B. The Stress Field

Duhamel's analogy states that the stress field in a body subjected to a temperature distribution,  $T(r, \theta)$ , but with zero body force and zero surface tractions is the same as that given by a superposition of hydrostatic pressure<sup>1</sup>

$$\sigma_r = \sigma_\theta = -\beta T, \quad \tau_{r\theta} = 0$$

with that given by another problem in which the same body is kept at a uniform reference temperature but subjected to a body force with components

$$F_r = -\beta \frac{\partial T}{\partial r}, \quad F_\theta = -\beta \frac{1}{r} \frac{\partial T}{\partial \theta}$$

<sup>1</sup>To satisfy equilibrium, the hydrostatic pressure field can be thought of as having body force components  $F_r = \beta (\partial T / \partial r)$  and  $F_\theta = \beta (\partial T / \partial \theta) / r$  and surface tractions having a normal component of  $-\beta T$ . Thus, the superposition with the second problem yields the original conditions (zero body force and surface tractions).

and with a surface traction with a normal component of  $\beta T$  where

$$\beta = \frac{\alpha E}{1 - 2\nu} \quad (25)$$

corresponds to plane strain and

$$\beta = \frac{\alpha E}{1 - \nu} \quad (26)$$

to plane stress.

The solution to this problem is solved by introducing the Airy stress function,  $\Phi$ , such that

$$\sigma_r = \frac{1}{r} \frac{\partial \Phi}{\partial r} + \frac{1}{r^2} \frac{\partial^2 \Phi}{\partial \theta^2} + \beta T \quad (27)$$

$$\sigma_\theta = \frac{\partial^2 \Phi}{\partial r^2} + \beta T \quad (28)$$

$$\tau_{r\theta} = -\frac{\partial}{\partial r} \left( \frac{1}{r} \frac{\partial \Phi}{\partial \theta} \right) \quad (29)$$

Stresses given in this manner automatically satisfy equilibrium. Compatibility is satisfied if

$$\nabla^4 \Phi = -\kappa \nabla^2 T \quad (30)$$

where

$$\kappa = \frac{\alpha E}{1 - \nu} \quad (31)$$

corresponds to plane strain and



$$\kappa = \alpha E \quad (32)$$

to plane stress.

The stresses associated with the Airy stress function must satisfy the modified traction boundary conditions:

$$\sigma_r = \beta T, \quad \tau_{r\theta} = 0 \text{ on } r = a, \quad -\pi < \theta < \pi \quad (33)$$

$$\sigma_\theta = \beta T, \quad \tau_{r\theta} = 0 \text{ on crack faces, } \theta = \pm \pi, \quad 0 < r < a \quad (34)$$

### 3.2 Solution

#### A. The Temperature Field

Applying Ohm's law, the heat flux induced by the current is

$$h(r, \theta) = \sigma \frac{a}{2r} (E_o/L)^2 \quad (35)$$

which yields the axisymmetric temperature distribution when Poisson's equation (21) is solved:

$$T(r, \theta) = \frac{\sigma}{k} \frac{a}{2} (E_o/L)^2 (a - r) + T_o \quad (36)$$

#### B. The Stress Field

From (30) and (36), the resulting nonhomogeneous biharmonic equation in plane strain becomes

$$\nabla^4 \Phi = \frac{\alpha E a}{2(1 - \nu)kr} (E_o/L)^2 \quad (37)$$

This equation is solved using superpositioning and separation of variables. The solution to this equation (for details, see Appendix A) is

$$\Phi = \frac{\alpha E}{2(1 - \nu)k} \left( \frac{E_o}{L} \right)^2 \frac{r^3}{a} (1 + \cos \theta) + \sum_{n=1}^{\infty} D_n r^{\lambda_n} \Omega_n \quad (38)$$

where  $\Omega_n$  are the symmetric Williams' eigenfunctions which yield the relationships

$$\begin{aligned}\sigma_r &= \sum_{n=1}^{\infty} D_n r^{(n-2)/2} \left[ (6-n)\cos(n-2) \frac{\theta}{2} + (n+2)(-1)^n \cos(n+2) \frac{\theta}{2} \right] \\ \sigma_\theta &= \sum_{n=1}^{\infty} D_n r^{(n-2)/2} \left[ (n+2)\cos(n-2) \frac{\theta}{2} - (n+2)(-1)^n \cos(n+2) \frac{\theta}{2} \right] \\ \tau_{r\theta} &= \sum_{n=1}^{\infty} D_n r^{(n-2)/2} \left[ (n-2)\sin(n-2) \frac{\theta}{2} - (n+2)(-1)^n \sin(n+2) \frac{\theta}{2} \right]\end{aligned}\quad (39)$$

### C. The Stress Intensity Factor, $K_1$

Obtaining a stress intensity factor requires finding the coefficients  $D_n$  which satisfy the appropriate boundary conditions. The boundary conditions (see Appendix A) require

$$\begin{aligned}\sum_{n=1}^{\infty} D_n a^{(n-2)/2} \left[ (6-n)\cos(n-2) \frac{\theta}{2} + (n+2)(-1)^n \cos(n+2) \frac{\theta}{2} \right] \\ = - \frac{\sigma a^2}{2k} \left( \frac{E_0}{L} \right)^2 \frac{aE}{9(1-\nu)} (3 + 2\cos\theta) \\ \sum_{n=1}^{\infty} D_n a^{(n-2)/2} \left[ (n-2)\sin(n-2) \frac{\theta}{2} - (n+2)(-1)^n \sin(n+2) \frac{\theta}{2} \right] \\ = - \frac{\sigma a^2}{2k} \left( \frac{E_0}{L} \right)^2 \frac{aE}{9(1-\nu)} (2 \sin\theta)\end{aligned}\quad (40)$$

The the stress intensity factor,  $K_1$ , is defined by

$$K_1 = \lim_{r \rightarrow 0} \sqrt{2\pi r} \sigma_\theta \text{ evaluated at } \theta = 0. \quad (41)$$

From (39),

$$K_1 = 4\sqrt{2\pi} D_1.$$

From Appendix A,

$$D_1 = \frac{-\sigma a^{5/2}}{2k} \left(\frac{E_0}{L}\right)^2 \frac{aE}{9(1-\nu)} (3d_1 + 2d_2) \quad (42)$$

where  $d_1$  and  $d_2$  refer to the normalized coefficients  $d_1^{(1)}$  and  $d_2^{(1)}$  which correspond respectively to unit pressure and sinusoidal loading on the boundary  $r = a$ .

Thus the stress intensity factor can be written generally as

$$K_1 = \frac{-2\sqrt{2\pi}}{9} \frac{aE\sigma}{k(1-\nu)} \left(\frac{E_0}{L}\right)^2 a^{5/2} [3d_1 + 2d_2] \quad (43)$$

for the plane strain case.

The generic coefficients  $d_1$  and  $d_2$  were determined numerically by least squares technique (see Appendix B). For this configuration,

$$\begin{aligned} d_1 &= 0.560764 \\ d_2 &= -0.913788 \end{aligned}$$

#### 4 RESULTS

The key results of the benchmark problem are the following two simple expressions which give estimates of the error in the steady state temperature and the associated thermally induced stress intensity factor:

$$T - T_o = \frac{\sigma}{2k} \left(\frac{E_0}{L}\right)^2 a^2 \quad (44)$$

$$K_1 = 0.231 \frac{aE\sigma}{2k} \left(\frac{E_0}{L}\right)^2 a^{5/2} \quad (45)$$

for Poisson's ratio equal to 0.3. Applying these results to the specific data generated by the thermal mechanical fatigue tests in reference 1, it is shown that the effect of the current on the local temperature, and consequently thermoelastic stress intensity factor, can be quite significant.

The materials used for high-pressure compressor and turbine disks and spacers in the Air Force F100 engine are high strength nickel-base alloys IN100 and Astroloy [1]. Fatigue data in [1] were provided for IN100. The temperature range of the tests is between 500 and 1200°F. Materials properties data for IN100 are listed in Table 2 for three temperatures: 70, 600 and 1200°F. Under the assumption that the sinusoidal variations of heat flux (current) and temperature are in phase (steady state thermal analysis), the maximum voltage corresponds to the maximum temperature. Thus, the 1200°F data were used for calculating the magnitude of K.

The stress intensity factor in the thermal-mechanical fatigue tests at termination, according to [1], is approximately 80 ksi  $\sqrt{\text{in.}}$ . A significant error, then, would be about 10 ksi  $\sqrt{\text{in.}}$  (> 10%). Using the above expression and a specimen length of 1.5 in, this degree of error would require an applied voltage of only 0.65 V (for a critical crack length of 0.3 in.). This small voltage prompted further investigation during which it was learned that the actual voltage drops measured across the test specimens were less than 0.4 V [27]. (Using the upper limit of the 0 - 3 V range quoted in [1] would yield an electric current-induced stress intensity in this material of greater than 150 ksi  $\sqrt{\text{in.}}$ !) Using a revised voltage range of 0 - 0.4 V and the materials data in Table 2, the most severe test conditions would yield a current induced stress intensity of approximately 3.5 ksi  $\sqrt{\text{in.}}$ . This value would not be expected to cause significant errors in the experimental methods that are presently used for measuring crack growth.

However, the expression for stress intensity factor is strongly dependent on crack length (as  $a^{5/2}$ ). Thus, a slight extension of the critical crack length can change the previously relatively small errors in K to significant ones. For example, extending the critical crack length from 0.3 in. to 0.4 in. results in an approximate 10% stress intensity error when the same upper limit on voltage (0.36 V) is applied.

The simple expression for current induced stress intensity presented above offers the advantage that it can easily be applied to different materials. Due to variations in materials properties, particularly electrical and thermal conductivity, small voltages may have pronounced effects on the electric current induced K for other materials.

Table 3 lists several commercially available high-strength nickel alloys and their compositions for comparison. Some of these alloys are used in gas turbine manufacture. Pertinent materials properties for each of these alloys are listed in Table 4. The room temperature and 600 °F data for IN100 were used to calculate stress intensity estimates for comparison to those materials listed in Table 4. The ratios of  $K$  to the appropriate temperature value of  $K$  for IN100 are also listed in the table. It is noted that the stress intensity estimates of all materials listed are greater than that of IN100. It is possible that the resistivity of IN100 as listed (calculated from data obtained during the fatigue testing) is greater than the actual value due to equipment configuration and testing error. This would suggest that the actual stress intensity error is significantly greater than the 5% previously stated, possibly even twice as high.

Displacements at the crack edge were calculated to compare with test observations. The detailed displacement analysis is given in [35]. The analysis reveals a small crack opening displacement of approximately 0.0001 in. These results are consistent with the crack opening displacements measured on test specimens.

## 5 DISCUSSION

The use of a benchmark or model problem to estimate errors in stress intensity factors and local temperatures in thermal-mechanical fatigue testing which uses large electric currents for heating has shown that this mode of testing results in a more severe stress state than if conventional heating methods are used. The reason for the more severe stress state is that the application of a constant voltage across a cracked specimen results in a singular current and, consequently, a singular heat source. The singular heat source does not result in a temperature singularity, however, so the temperature remains bounded at the crack tip.

The relative discrepancy between conventional heating fatigue testing and resistance heating fatigue is quite dependent on crack size (as  $a^{5/2}$ ) and materials properties: primarily thermal and electrical conductivity and linear thermal expansion. Materials exhibiting low electrical resistance and high thermal expansion are, in general, more susceptible to this mode of thermal loading.

Simple expressions for estimating the contribution of electric current to the stress intensity factor and local temperature field were developed. These expressions are estimates in light of some basic assumptions made during problem formulation. The validity and consequence of some of these assumptions will be discussed here.

Beginning with the electric potential problem, we first assumed that skin effects (the concentration of electric current near surfaces) can be neglected. This allows the problem to be configured as one in two-dimensional plane strain. In reality, however, the skin effect is known to be important in some cases. If the skin effect is important in the present system the consequence is a hotter surface due to the higher current density in that area. One example where the skin effect is important is in a cracked plate with uniform applied magnetic field [34]. The increase in current density uniformly from the center to the outer edge in this case was determined by finite element to be approximately 20%. It is possible that this edge effect may be related to the shear lip formation observed in some of the fatigue specimens in that  $K$  could be higher near the surfaces of the specimens.

Secondly, the assumption that higher order terms in the electric potential series expression can be neglected when calculating the heat source induces an error when calculating the stress intensity factor. The trouble with including more than a limited number of terms in the series is that the problem would then have to be solved completely numerically. By using the current approach, relatively simple expressions were derived for the temperature error and the current induced stress intensity which may be easily evaluated for any material. However, these results are not exact and only provide an estimate of the magnitude of this effect.

It is noted again that although the greater crack growth rates are observed in the in-phase testing, it is the out-of-phase test samples that exhibit the anomalous crack growth behavior. Time histories of temperature and electric current that were taken during a crack growth test [27] are plotted in Figure 5. It is apparent from this data that the assumption that the current and the temperature are in phase is inappropriate under actual test conditions. In fact, it is clear from the phase lag between current and temperature that thermal transients play an important role in these cases. Moreover, the temperature information in the figure may be used to estimate the relative magnitude of the time dependent term in the heat equation. Averaging over a circle of radius  $a$ , the heat flux generated by the electric current ( $15^{\circ}\text{F/sec}$ ) is of comparable magnitude to the thermal transient term ( $12^{\circ}\text{F/sec}$ ). This indicates that the assumption of steady state in the thermal analysis should be reconsidered and that transient thermal effects should be taken into consideration in order to accurately relate analyses to the laboratory situation.

In conclusion, a first estimate to the role of electric current in thermal fatigue tests has been obtained. It was calculated under the assumption that the singular heat flux

term would dominate the near field behavior at the crack tip. Appropriate linear differential equations were solved analytically up to the point in the thermoelastic problem where the boundary conditions had to be satisfied. A numerical technique based on a least squares approach was used to satisfy these constraints.

Since little work has been done in this area the resulting solution is fundamental in that it may be easily used to establish thermal stresses for a variety of test configurations. Consequently, it may be readily utilized to assess the validity of thermal mechanical testing procedures which incorporate resistance heating and neglect thermoelastic stresses.

## REFERENCES

1. D. A. Wilson and J. R. Warren, "Thermal mechanical crack growth rate of a high strength nickel base alloy," ASME Transactions, paper no. 85-GT-12, 30th International Gas Turbine Conference and Exhibit, Houston, TX, March 18-21, 1985.
2. H. H. Johnson, "Calibrating the electrical potential method for studying slow crack growth," *Mat. Res. & Stds.*, 5 (1965) 442-445.
3. G. Clark and J. F. Knott, "Measurement of fatigue cracks in notched specimens by means of theoretical electrical potential calibrations," *J. Mech. Phys. Solids*, 23 (1975) 215-216.
4. R. O. Ritchie and K. J. Bathe, "On the calibration of the electrical potential technique for monitoring crack growth using finite elements," *Int. J. Fract.*, 15 (1979) 47-58.
5. M. A. Hicks and A. C. Pickard, "A comparison of theoretical and experimental methods for calibrating the electric potential drop technique for crack determination," *Int. J. Fract.*, 20 (1982) 91-101.
6. M. Saka and H. Abe, "A path-independent integral for 2-dimensional cracks in homogeneous isotropic conductive plate," *Int. J. Engng. Sci.*, 21 (1983) 1451-1457.
7. F. B. Hildebrand, *Advanced Calculus for Applications*, Prentice-Hall, Inc. (1976) p. 647.
8. Y. C. Fung, *Foundations of Solid Mechanics*, Prentice-Hall, Inc. (1965) p. 389.
9. H. Parkus, *Thermoelasticity*, Blaisdell Pub. Co. (1968) pp. 24-44.
10. B. A. Boley and J. A. Weiner, *Theory of Thermal Stresses*, John Wiley & Sons (1960) pp. 101-116.
11. A. L. Florence and J. N. Goodier, "Thermal Stresses due to disturbance of uniform heat flow by an insulated ovaloid hole," *J. Appl. Mech.*, 27 (1960) 635-639.
12. G. C. Sih, "On the singular character of thermal stresses near a crack tip," *J. Appl. Mech.*, 29 (1962) 587-589.
13. G. R. Irwin, "Fracture," in *Handbuch der Physik*, vol. VI, S. Fluegge, ed., Springer-Verlag (1958) pp. 551-589.
14. S. P. Timoshenko and J. N. Goodier, *Theory of Elasticity*, McGraw-Hill Book Co. (1970) p. 67.
15. M. N. Bapu Rao, "Thermal Stress around an insulated crack in an infinite plate subjected to uniform heat flow," *Int. J. Fract.*, 12 (1976) 777-779.



16. P. J. Torvik, "Application of an eigenfunction expansion to the determination of stress-intensity factors," ASME Trans., paper no. 77-WA/GT-1, Winter Annual Meeting, Atlanta, GA, November 27-December 2, 1977.
17. P. J. Torvik, "On the determination of stresses, displacements and stress intensity factors in edge-cracked plates with mixed boundary conditions," J. Appl. Mech., 46 (1979) 611-617.
18. M. Svoboda, "Experimental results on the influence of thermal stresses on the stability of a crack," Int. J. Fract., 5 (1969) 315-325.
19. Y. Konishi and A. Atsumi, "The linear thermoelastic problem of uniform heat flow disturbed by a two-dimensional crack in a strip," Int. J. Engng. Sci., 11 (1973) 1-7.
20. H. Sekine, "Thermal Stress singularities at tips of a crack in a semi-infinite medium under uniform heat flow," Engng. Fract. Mech., 7 (1975) 713-729.
21. H. Sekine, "Thermal stresses near tips of an insulated line crack in a semi-infinite medium under uniform heat flow," Engng. Fract. Mech., 9 (1977) 499-507.
22. H. Sekine, "Crack problem for a semi-infinite solid with heated bounding surface," J. Appl. Mech., 44 (1977) 637-642.
23. J. Tweed and S. Lowe, "The thermoelastic problem for a half-plane with an internal line crack," Int. J. Engng. Sci., 17 (1979) 357-363.
24. K. Herrmann and K. Kuemmerling, "A crack-thermal stress problem in a doubly connected solid," Arch. Mech., 28 (1976) 171-188.
25. P. A. Gradin, "A note on the J-integral for thermal stress crack problems," Int. J. Fract., 23 (1985) R59-R50.
26. N. Sumi and T. Katayama, "Thermal stress singularities at tips of a Griffith crack in a finite rectangular plate," Nucl. Engng. Des., 60 (1980) 389-394.
27. Personal communication, J. R. Warren, P&WA, April 1985.
28. S. L. Hoyt, ed., *Metals Properties*, ASME Handbook, McGraw-Hill Book Co., Inc. (1954) 371-383.
29. *Monel, Inconel, Nickel and Nickel Alloys*, International Nickel Co., Inc. (1947) 14-17.
30. H. C. Cross and W. F. Simmons, "Heat resisting metals for gas turbine parts," Symposium on materials for gas turbines, 49th Annual Meeting, ASTM, June 24-28, 1946, Buffalo, NY (1947) 3-51.
31. D. W. Grobecker, ed., *Metals for Supersonic Aircraft and Missiles*,

Proceedings of the Conference Heat Tolerant Metals for Aerodynamic Applications, ASM, January 28-29, 1957, Albuquerque, NM (1958) 234-249.

32. *Source Book on Industrial Alloy and Engineering Data*, American Society for Metals, (1978) 311-337.
33. T. Lyman, ed., *Metals Handbook*, vol. 1, "Properties and Selection of Metals," American Society for Metals, 1978.
34. G. Yagawa and T. Horie, "Cracked beam under influence of dynamic electromagnetic force," *Nuclear Engrg. and Des.*, 69 (1982) 49-55.
35. S. E. Cunningham, "An Estimate of the Thermoelastic Stress Field Induced by an Electric Current Flowing Around a Crack," Report SM-85-16, Department of Mechanical Engineering, Carnegie-Mellon University, Pittsburgh, Pennsylvania (1985).

**Table 1**  
**Electric Potential Coefficient Values**

Coefficient Number (n)	Value (A <sub>n</sub> )
0	.970527300
1	1.414210000
2	.341726000
3	-.353554000
4	-.341728200
5	-.044193700
6	.069035320
7	-.011048700
8	-.054572040
9	-.003452562
10	.028407400
11	-.001208524
12	-.021641700
13	-.000453151
14	.014980200
15	-.000178091
16	-.011750900
17	-.000072299
18	.009123044
19	-.000030232
20	-.007432150
21	-.000012750
22	.006108524
23	-.000005576
24	-.005137681
25	-.000002395
26	.004368960
27	-.000001079
28	-.003766370
29	-.000000430
30	.003277960
31	-.000000251
32	-.002879890

Notes:

$$E = C_o + \sum_{n=1}^{32} C_n r^{n/2} \cos \frac{n(\theta - \pi)}{2}$$

$$C_n = A_n \frac{E_o}{L} a^{(2-n)/2} \text{ for } n = 0, 1, 2, 3, \dots$$

e.g.,

$$C_o = 0.9705273 \frac{E_o a}{L}, \quad \frac{E_o}{L} \text{ in volts/in; } C_1 = \sqrt{2a} \frac{E_o}{L}$$

Table 2  
Properties of IN100

Temperature (°F)	Linear Thermal Expansion Coefficient, from 70° (10 <sup>-6</sup> in/in/°F)	Thermal Conductivity Btu-in/hr-ft <sup>2</sup> -°F)	Electrical Resistivity (μΩ-cm)	Young's Modulus (10 <sup>6</sup> psi)
RT	6.8 <sup>(1,2)</sup>	80 <sup>(1)</sup>	195 <sup>(2,3)</sup>	29.5 <sup>(1)</sup>
600	7.5 <sup>(1)</sup>	100 <sup>(1)</sup>	208 <sup>(3)</sup>	27.0 <sup>(3)</sup>
1200	8.0 <sup>(1)</sup>	130 <sup>(1)</sup>	220 <sup>(2,3)</sup>	24.0 <sup>(2,3)</sup>

Notes:

1. *Aeronautical Vest-pocket Handbook*, P&WA Publication, July 1979, p. 106-107.
2. Extrapolated.
3. Calculated from data obtained from J. Warren.

**Table 3**  
**Major Constituents of High Strength Nickel Alloys**

Material	Ni	Cr	(%) Co	Fe	Other	Reference
IN100	55	12.4	18.5	0.3	(3Mo,4 Ti,5Al)	1
Nickel	100	--	--	--	--	28
K Monel	63-70	--	--	2.0	(~ 25 Cu)	28,29
Monel	63-70	--	--	2.5	(~ 30 Cu)	28,29
Hastelloy B	60	1	--	6.0	(28 Mo)	28-30
Hastelloy C	60	16	--	--	(18Mo,4W)	28-31
"Inconel"	72	16	--	8		28-31
Inconel 600	(Ni+Co)=72	16	--	8		32
Inconel 718	55	19	1	15	(5 Nb)	32
Inconel X750	(Ni+Co)=70	15	--	6.5		32
Incoloy 800	33	21	--	42		32

Table 4  
Materials Properties of Several Nickel-Base Alloys

Material	Linear Thermal Expansion Coefficient ( $10^{-6}$ in/in/ $^{\circ}$ F)	Electrical Resistivity ( $10^{-6}$ $\Omega$ -cm)	Thermal Conductivity (Btu-in/in-ft <sup>2</sup> - $^{\circ}$ F)	Young's Modulus ( $10^6$ psi)	Temp. ( $^{\circ}$ F)	$K/K_{IN}^2$
Ni	7.4	6.84	637	30	70	3.9
K Monel	7.8	58.3	130	26	70	2.0
Monel	7.8	48.2	173	26	70	1.89
Hastelloy B	5.5	135	78.2	28.5	70	1.16
Hastelloy C	6.3	133	86.9	28.5	70	1.21
Inconel	6.4	98.1	104	31	70	1.51
Inconel 600	5.8	103	103	30	70	1.28
	7.9	107	133	27.5	600	1.57
	8.6	113	172	24.8	1200	1.6
Inconel 718	7.8	125	77	29	70	1.83
	8.0	129	111	26.7	600	1.53
	8.6	134	147	23.7	1200	1.54
Inconel X750	6.9	121	83	31	70	1.66
	7.5	126	109	(28.5)	600	1.6
	8.4	131	143	25.5	1200	1.2
Incoloy 800	8.7	98.8	80	28.4	70	2.4
	9.0	111	115	25.4	600	1.8
	9.6	124	152	22.3	1200	1.6

$K_{IN}^2$  refers to the stress intensity factor calculated for IN100.

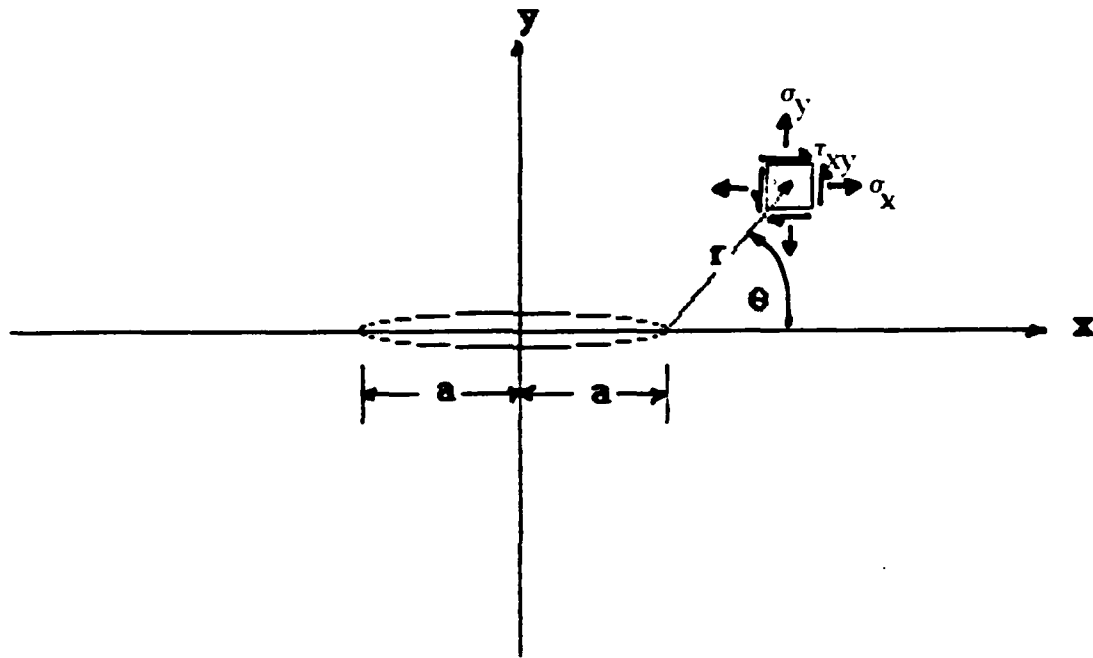


Figure 1. Thermal Stress Component Geometry Near Crack

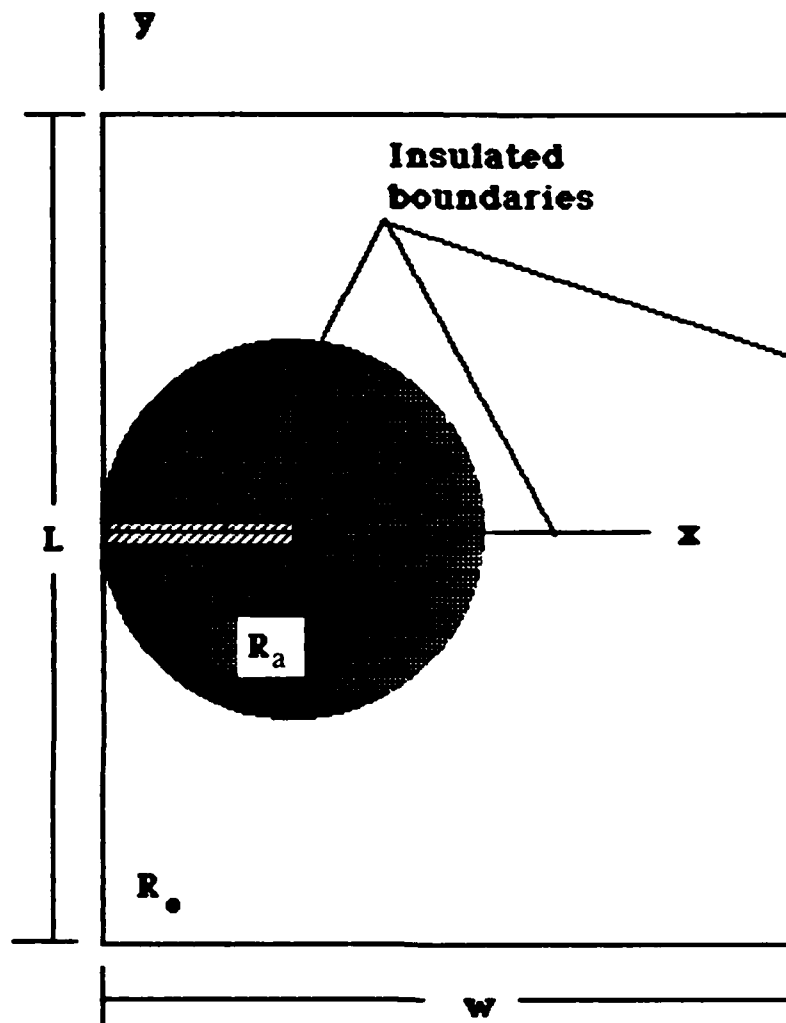


Figure 2. Benchmark Problem Geometry



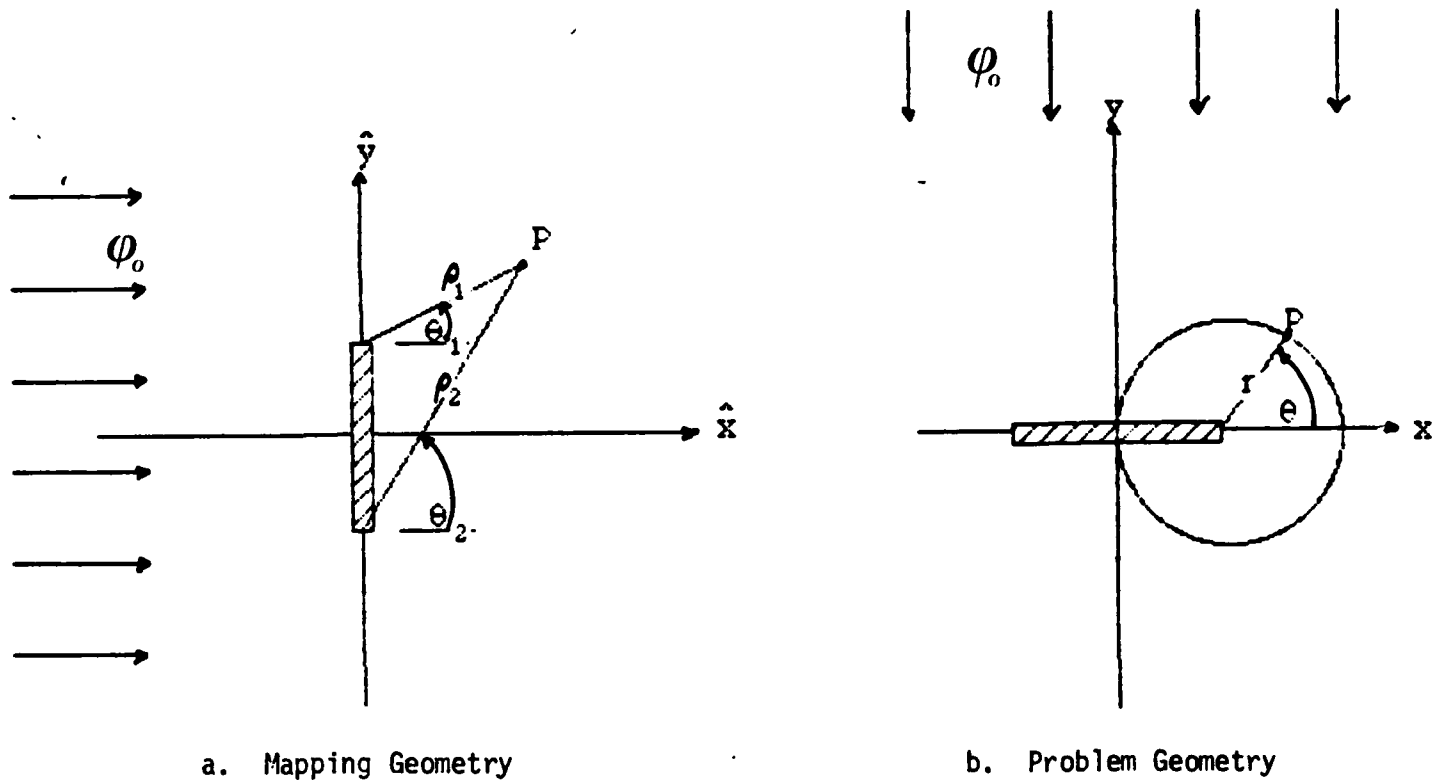


Figure 3. Relation of Schwarz-Christoffel Mapping Geometry to the Problem Geometry

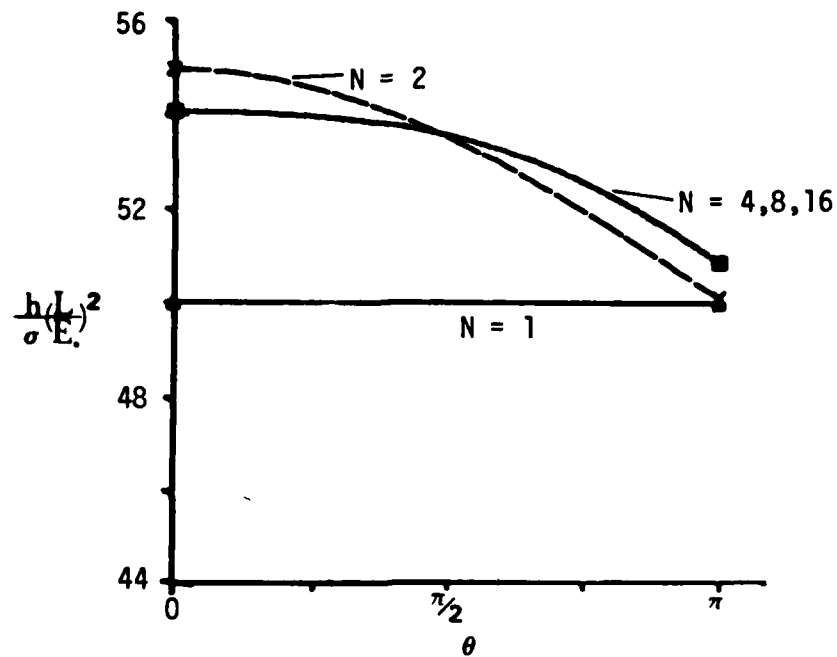
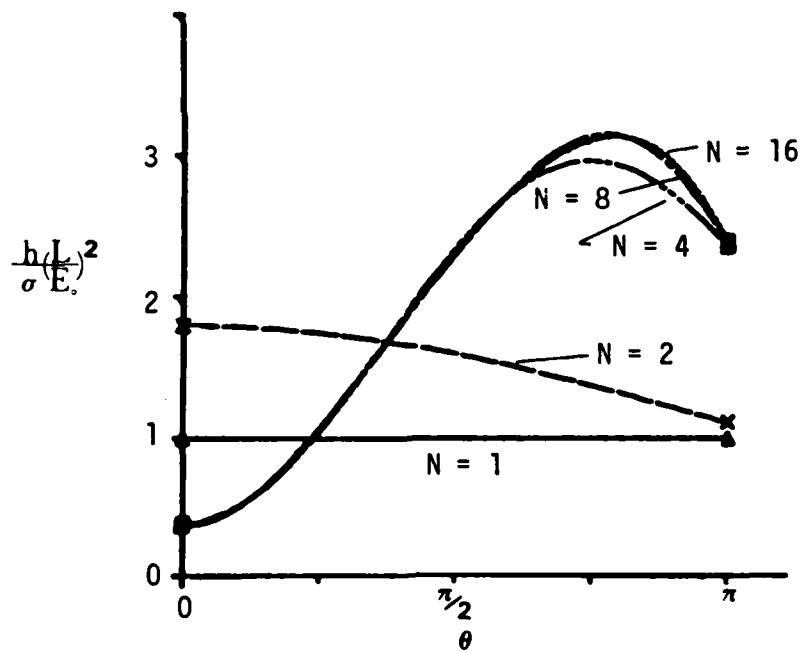
a) at  $r = 0.01a$ b) at  $r = a/2$ 

Figure 4. Heat as a Function of Position for Various Numbers of Terms in the Fourier Cosine Series

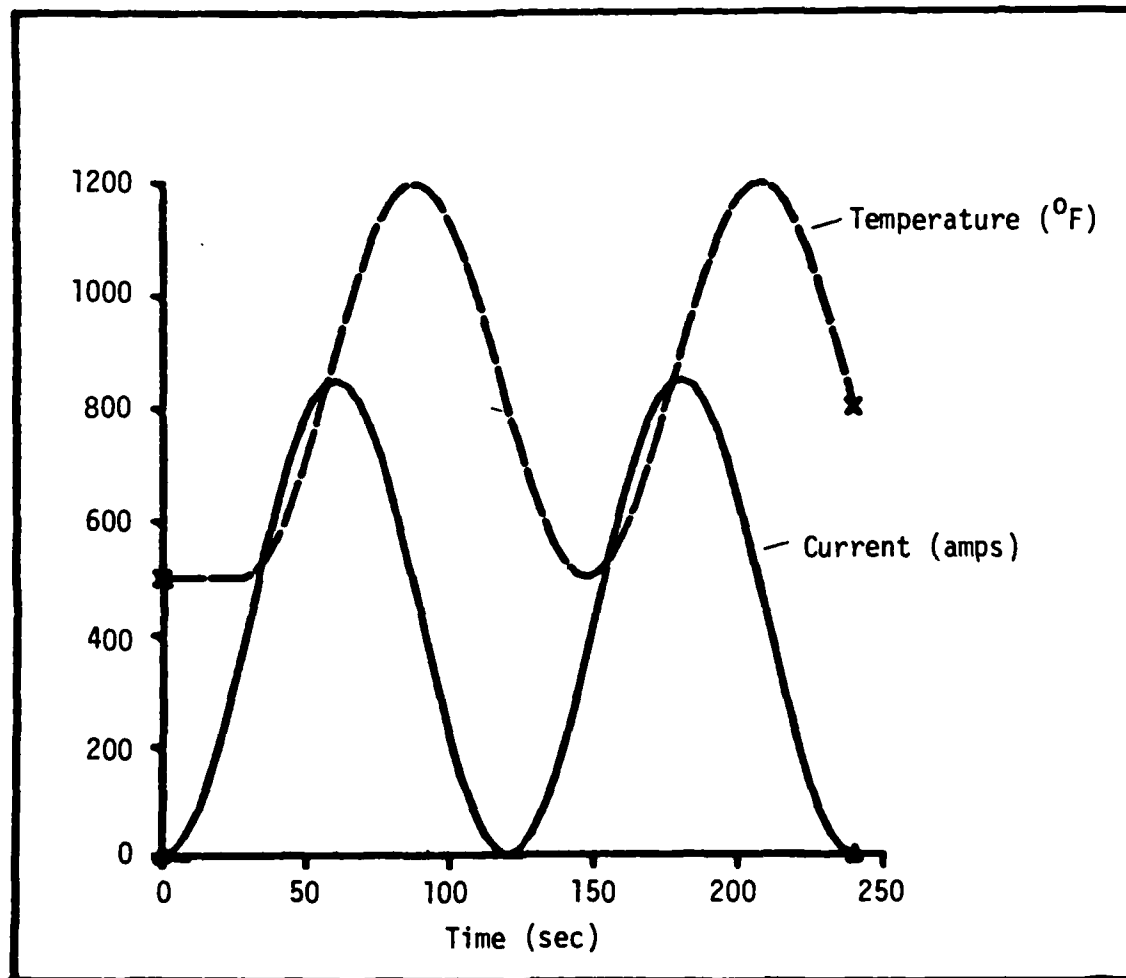


Figure 5. Time History of Temperature and Electric Current Measured During Crack Growth Tests

## **APPENDICES**

## Appendix A

## DETAILS OF THE THERMOELASTIC SOLUTION

From

$$\nabla^4 \Phi = \frac{-\alpha E}{(1 - \nu)} \nabla^2 T$$

and

$$\nabla^2 T = - \frac{\sigma}{2k} \left( \frac{E_0}{L} \right)^2 \frac{a}{r},$$

the governing equation can be written as

$$\nabla^4 \Phi = \frac{\sigma \alpha E}{2k(1 - \nu)} \left( \frac{E_0}{L} \right)^2 \frac{a}{r} \equiv \frac{B}{r}$$

where  $\Phi$  must satisfy the traction conditions of (33) and (34). Using the principle of linear superposition, let

$$\Phi = \Phi_H + \Phi_P$$

where  $\Phi_P$  is the particular solution satisfying

$$\nabla^4 \Phi_P = \frac{B}{r},$$

and  $\Phi_H$  is the homogeneous solution satisfying

$$\nabla^4 \Phi_H = 0.$$

A solution for  $\Phi_P$  is

$$\Phi_P = \frac{Br^3}{9}$$

The homogeneous solution,  $\Phi_H$  can also be broken into component parts:

$$\Phi_H = \Phi_{H1} + \Phi_{H2}$$

where  $\Phi_{H2}$  is the Williams' eigenfunction solution ( $\Phi_{H2}$  automatically satisfies (34) and its coefficients are numerically determined such that (33) is satisfied in a least squares sense) while  $\Phi_{H1}$  frees up the crack faces from the tractions imposed by  $\Phi_p$ .

By separation of variables, an expression for  $\Phi_{H1}$  is:

$$\Phi_{H1} = \frac{Br^3}{9} \cos \theta$$

It is noted that the combination  $\Phi_p + \Phi_{H1}$  satisfies the crack face conditions:

$$\sigma_\theta = \frac{\partial^2 \Phi}{\partial r^2} + \beta T = \beta T \text{ at } \theta = \pm \pi$$

$$\tau_{r\theta} = -\frac{\partial}{\partial r} \left( \frac{1}{r} \frac{\partial \Phi}{\partial \theta} \right) = 0 \text{ at } \theta = \pm \pi$$

The appropriate boundary conditions for  $\Phi_{H2}$  are derived from

$$a) \sigma_r \Big|_{r=a} = \left( \frac{1}{r} \frac{\partial}{\partial r} + \frac{1}{r^2} \frac{\partial^2}{\partial \theta^2} \right) [\Phi_p + \Phi_{H1} + \Phi_{H2}] + \beta T = \beta T$$

or, after incorporating the above expressions for  $\Phi_p$  and  $\Phi_H$  and evaluating at  $r = a$ ,

$$\frac{1}{r} \frac{\partial \Phi_{H2}}{\partial r} + \frac{1}{r^2} \frac{\partial^2 \Phi_{H2}}{\partial \theta^2} \Big|_{r=a} = -\frac{Ba}{9} (3 + 2\cos \theta)$$

and

$$b) \tau_{r\theta} \Big|_{r=a} = -\frac{\partial}{\partial r} \left[ \frac{1}{r} \frac{\partial}{\partial \theta} (\Phi_p + \Phi_{H1} + \Phi_{H2}) \right] = 0$$

or,

$$-\frac{\partial}{\partial r} \left( \frac{1}{r} \frac{\partial \Phi_{H2}}{\partial \theta} \right) = -\frac{2}{9} Ba \sin \theta$$

Thus, the Williams' eigenfunction solution must satisfy boundary conditions of the form:

$$\sigma_r \Big|_{r=a} = -\frac{Ba}{9} (3 + 2\cos\theta)$$

$$\tau_{r\theta} \Big|_{r=a} = -\frac{Ba}{9} 2 \sin\theta$$

In order to generalize and further simplify the numerical evaluation of coefficients,  $D_n$ , in the eigenfunction solutions,  $\Phi_{H2}$ , these coefficients can be expressed as the sum of normalized coefficients  $d_1^{(n)}$  and  $d_2^{(n)}$  which correspond to unit pressure and sinusoidal loadings, respectively, on the boundary  $r = a$ . In other words, if on the boundary  $r = a$ ,

$$(\sigma_r)_1 = \sum_{n=1}^{\infty} d_1^{(n)} \chi_n(\theta) = 1, \quad (\tau_{r\theta})_1 = \sum_{n=1}^{\infty} d_1^{(n)} \gamma_n(\theta) = 0,$$

and

$$(\sigma_r)_2 = \sum_{n=1}^{\infty} d_2^{(n)} \chi_n(\theta) = \cos\theta, \quad (\tau_{r\theta})_2 = \sum_{n=1}^{\infty} d_2^{(n)} \gamma_n(\theta) = \sin\theta,$$

For  $\chi_n(\theta)$  and  $\gamma_n(\theta)$  representing the Williams' eigenfunction series for  $\sigma_r$  and  $\tau_{r\theta}$ , respectively, the coefficients  $D_n$  in (40) are such that

$$D_n a^{(n-2)/2} = -\frac{Ba}{9} (3d_1^{(n)} + 2d_2^{(n)}), \quad n = 1, 2, \dots, \infty.$$

Numerical calculation of  $d_1^{(n)}$  and  $d_2^{(n)}$  is discussed in Appendix B.

Substituting for  $B$  and dividing by  $a^{-1/2}$ , the singular coefficient,  $D_1$ , becomes

$$D_1 = -\frac{\sigma}{2k} a^{5/2} \left(\frac{E_0}{L}\right)^2 \frac{aE}{9(1-\nu)} (3d_1^{(1)} + 2d_2^{(1)}).$$

## Appendix B

## METHOD OF LEAST SQUARES: CALCULATIONS AND CONVERGENCE CHECKS

The method of least squares was used to determine the coefficients  $d_1^{(n)}$  and  $d_2^{(n)}$  so that the appropriate boundary conditions presented in Appendix A are satisfied. The least squares method constructs a series representation which fits the boundary conditions over the interval of interest with a minimum of error. If the boundary conditions are written

$$\sigma_r = f(\theta), \tau_{r\theta} = g(\theta) \text{ on } r = a,$$

the error involved in summing  $\sigma_r$  and  $\tau_{r\theta}$  at the boundary  $r = a$  is<sup>3</sup>

$$\epsilon = \int_0^\pi \left\{ \left[ f(\theta) - \sum_{n=1}^{\infty} d_n \psi_n(\theta) \right]^2 + \left[ g(\theta) - \sum_{n=1}^{\infty} d_n \gamma_n(\theta) \right]^2 \right\} d\theta$$

where  $\psi_n(\theta)$  and  $\gamma_n(\theta)$  represent the Williams' eigenfunction series for  $\sigma_r$  and  $\tau_{r\theta}$  respectively.

In order to minimize  $\epsilon$  with respect to each coefficient  $d_n$ , take

$$\begin{aligned} \frac{\partial \epsilon}{\partial d_m} = 0 = & \int_0^\pi \left\{ -2 \left[ f(\theta) - \sum_{n=1}^{\infty} d_n \psi_n(\theta) \right] \psi_m(\theta) \right. \\ & \left. - 2 \left[ g(\theta) - \sum_{n=1}^{\infty} d_n \gamma_n(\theta) \right] \gamma_m(\theta) \right\} d\theta \end{aligned}$$

or,

$$\int_0^\pi [f(\theta) \psi_m + g(\theta) \gamma_m(\theta)] d\theta = \sum_{n=1}^{\infty} d_n \int_0^\pi (\psi_n \psi_m + \gamma_n \gamma_m) d\theta$$

If the array  $l_{nm}$  is defined as

<sup>3</sup>The calculations must be performed separately for the unit pressure and sinusoidal loading conditions. The method in the text describes the general procedure to be followed in both cases. For ease of notation, we have used  $d_n$  in place of either  $d_1^{(n)}$  or  $d_2^{(n)}$  in this appendix.



$$I_{nm} = \int_0^{\pi} (\psi_n \psi_m + \gamma_n \gamma_m) d\theta$$

and the constraint vector components as

$$F_m = \int_0^{\pi} (f(\theta) \psi_m + g(\theta) \gamma_m) d\theta$$

Then the error is minimized in a least squares sense if

$$\sum_{n=1}^N d_n I_{nm} = F_m \quad \text{as } N \rightarrow \infty$$

This equation can be solved for the unknown coefficients  $d_n$  for various values of  $N$  using a standard LU-decomposition method.

To check the numerical convergence, three tests were performed:

1. Stresses and errors were evaluated when functions  $f = 1$ ,  $g = \sin 2\theta$  were inputted. Results for the cases  $N = 4$  and  $N = 16$  are plotted in Figures B-1 and B-2 along with the known functions for comparison. Excellent correspondence between the known functions and the series representations for  $N = 16$  is noted, while the case  $N = 4$  still results in rather large error values.
2. The coefficients were calculated for a test case in which the exact coefficients were known. These were used to generate boundary conditions to see if the same coefficients were rendered. Results are tabulated in Table B-1 and show error values on the order of  $10^{-5}$ .
3. The coefficients were used to compute the boundary stresses to compare with the theoretical boundary conditions. Figures B-3 and B-4 show the results for four values of  $N$ . The results show that the boundary conditions are satisfied quite well for  $N$  as small as 16. Excellent agreement is noted for higher values of  $N$ .

The convergence checks illustrate quite rapid convergence and excellent behavior of the functions with approximately zero error accomplished with as low as 32 coefficients.

Table B-1

## NUMERICAL CONVERGENCE CHECK #2

	Crack Size = .075		Crack Size = 0.1	
	Input Values	Output Values	Input Values	Output Values
$d_1$	2.486730	2.486710	4.420850	4.420810
$d_2$	1.313280	1.313270	2.334720	2.334700
$d_3$	-5.091920	-5.091870	-9.052300	-9.052190
$d_4$	0.383660	0.383655	0.682062	0.682052

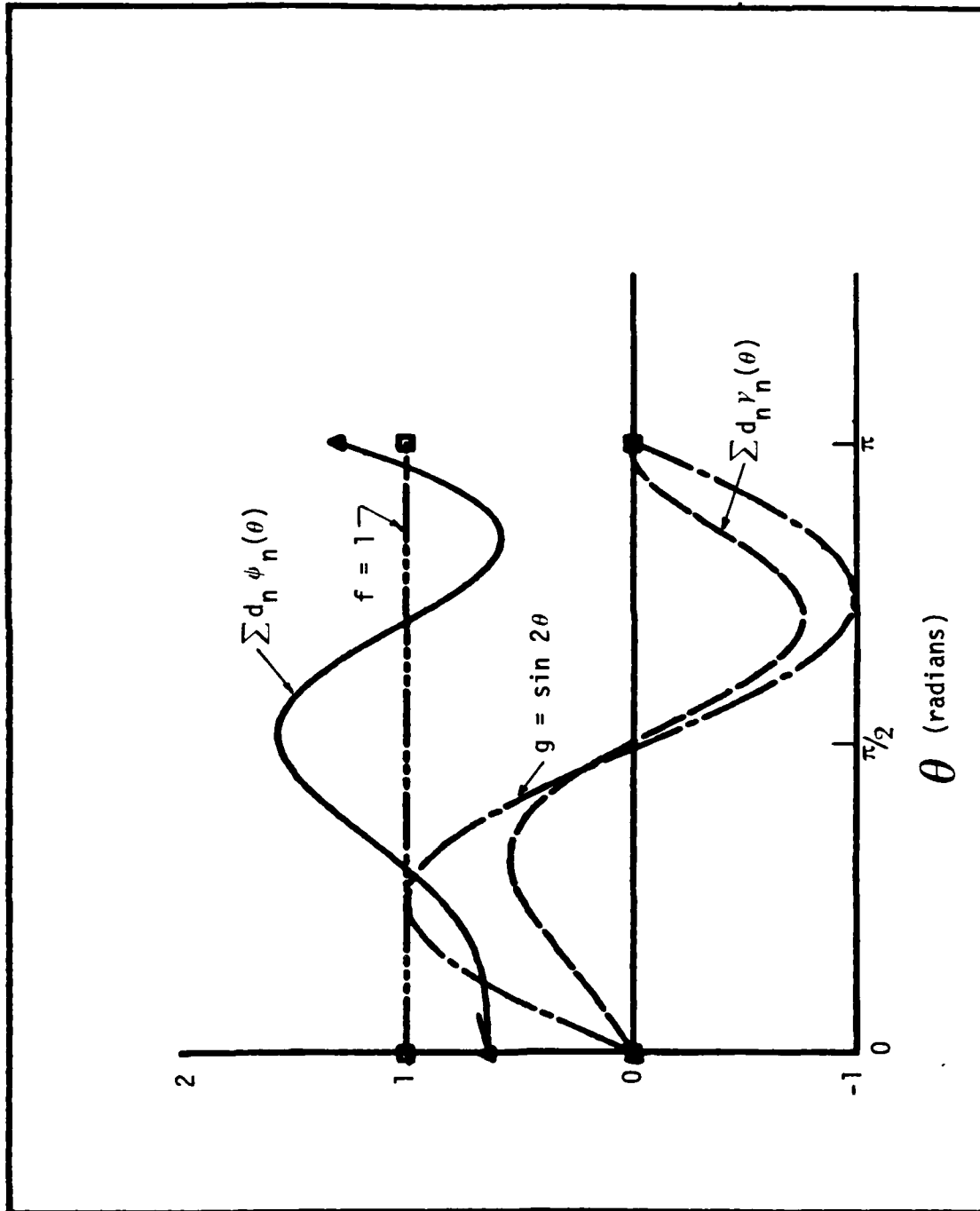


Figure B-1. Convergence Check #1: Least Squares Approximation for  $N = 4$

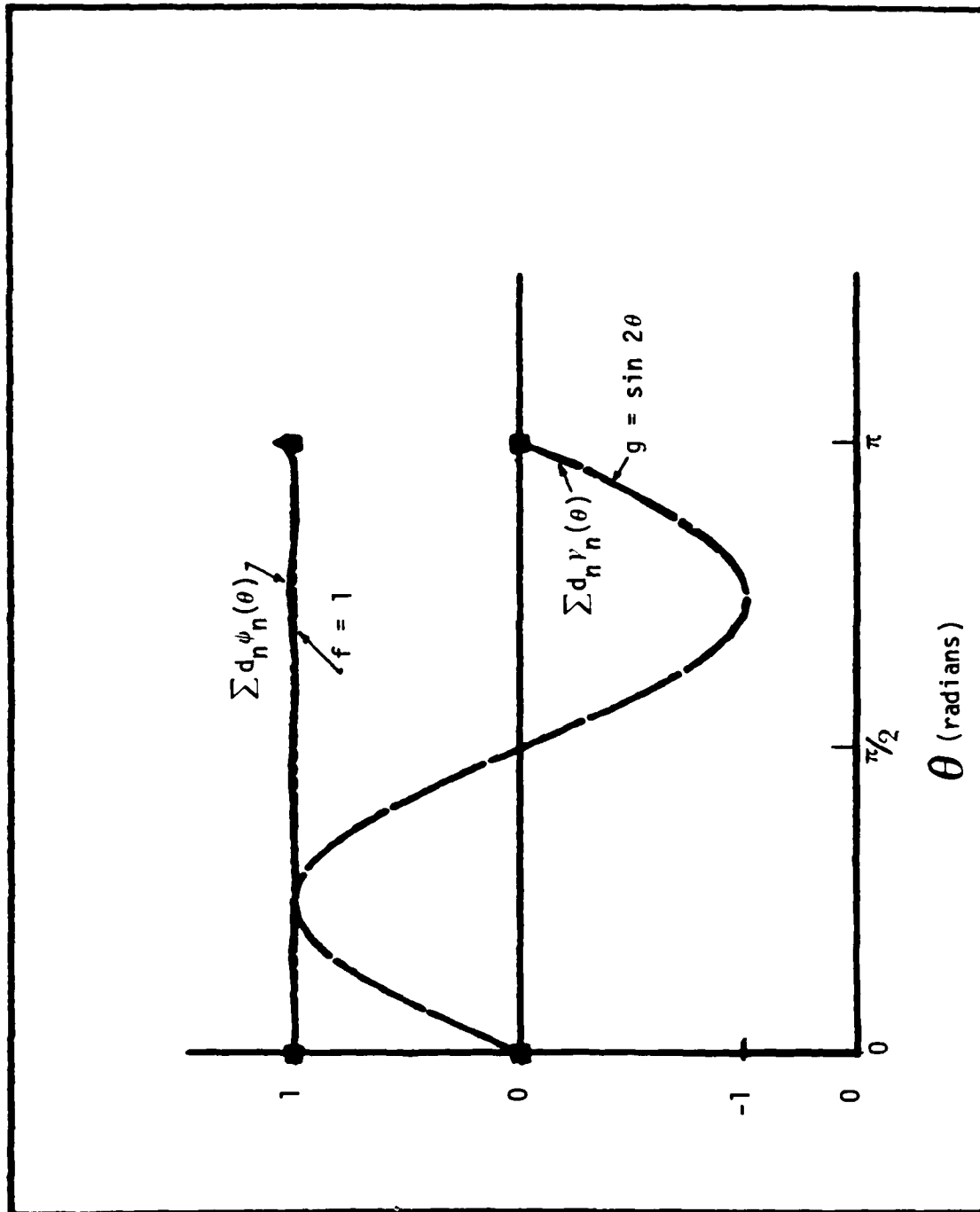


Figure B-2. Convergence Check #1: Least Squares Approximation for  $N = 16$

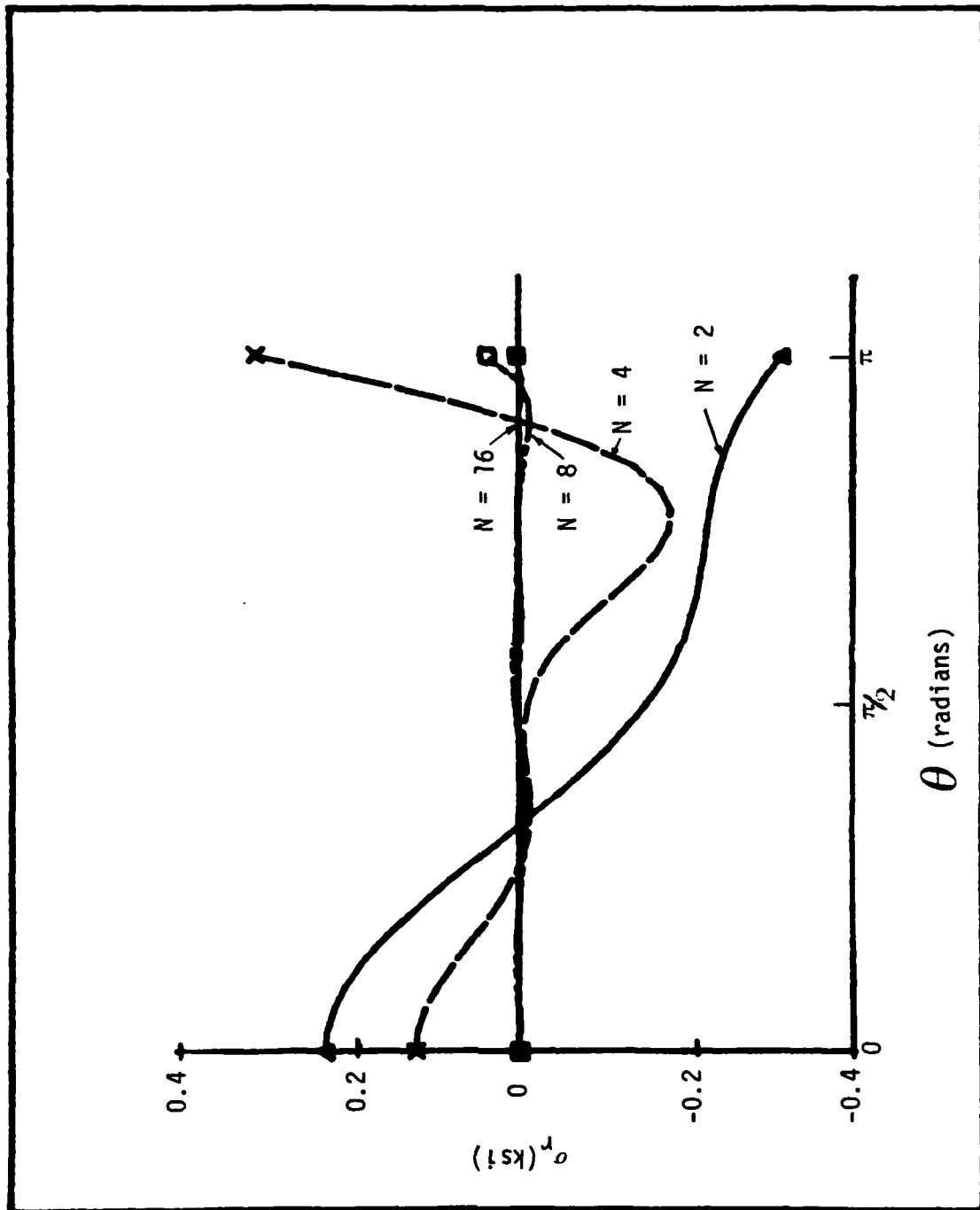


Figure B-3. Solution Check:  $\sigma_r$  at Boundary  $r = a$  for Various Values of  $N$

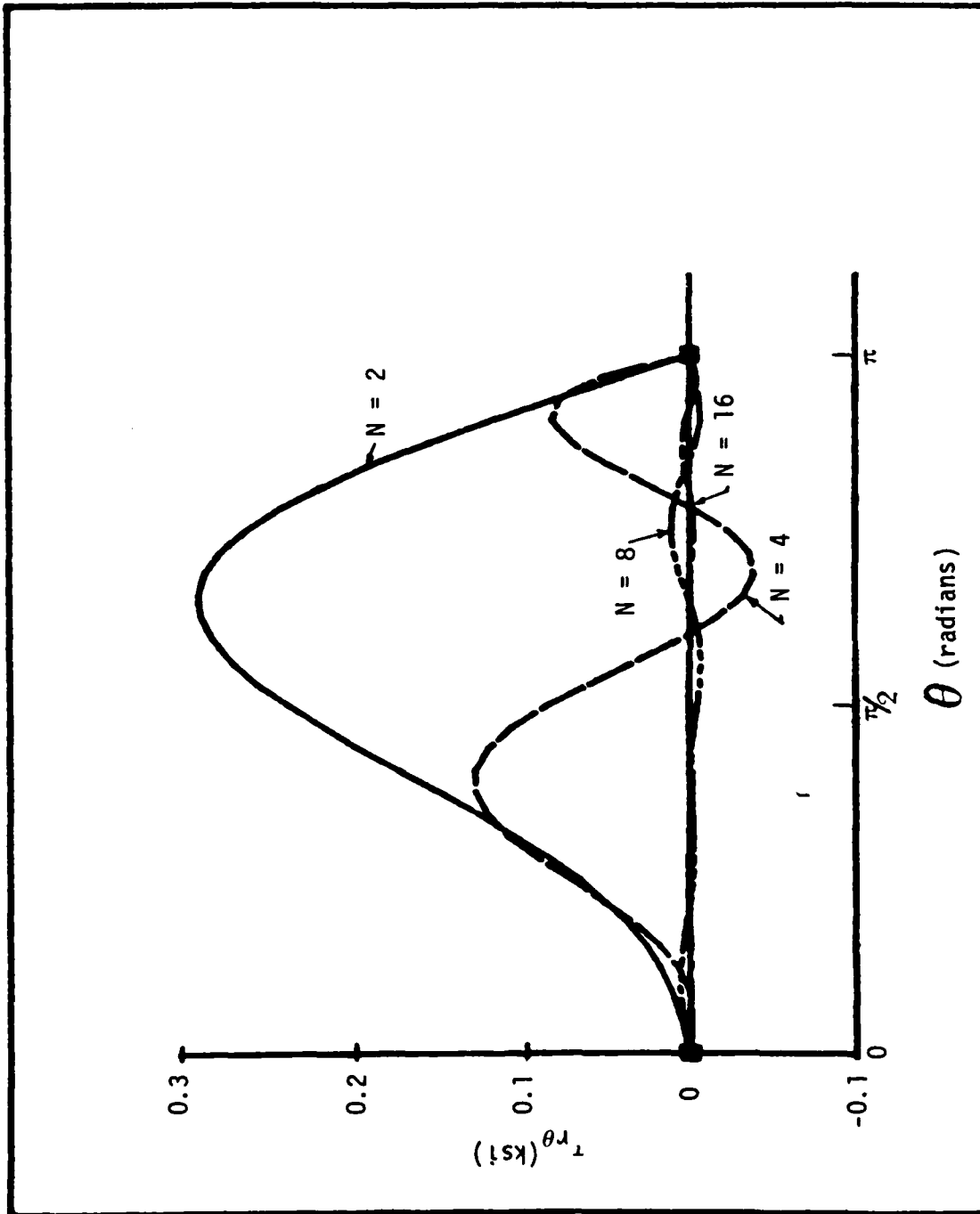


Figure B-4. Solution Check:  $\tau_{r\theta}$  at Boundary  $r = a$  for Various Values of  $N$

END

11-86

DT/C